

Transformation of trigonal planar B₄ into zigzag B₄ units within the new boride series Ti_{2-x}M_{1+x-δ}Ir_{3+δ}B₃ (x = 0.5 for M = V-Mn, x = 0 for M = Mn-Ni and δ < 0.2)

Jan P. Scheifers,^{# a} Michael Küpers,^{# b} Yuemei Zhang,^c Laura Lutz-Kappelman,^d Gordon J. Miller,^d
Boniface P. T. Fokwa^{* a}

-
- [a] Department of Chemistry
University of California, Riverside
Riverside, CA 92521, USA
*: E-mail: bfokwa@ucr.edu
#: co-first authors
- [b] Institute of Inorganic Chemistry
RWTH Aachen University
Aachen, D-52056, Germany
- [c] Department of Chemistry
Warren Wilson College
Asheville, NC 28815, USA
- [d] Department of Chemistry
Iowa State University
Ames, IA 50011, USA

Abstract

In metal-rich borides, numerous boron fragments B_n (n = 2, 3, 4, 5, 6) have been discovered, the B₄ units being the most versatile with four different shapes (bent, zigzag, trigonal planar and tetrahedral). We report on the new boride series Ti_{2-x}M_{1+x-δ}Ir_{3+δ}B₃ (x = 0.5 for M = V-Mn, x = 0 for M = Mn-Ni and δ < 0.2), in which a structural change occurs by successive substitution of the 3d transition metal M = V, Cr, Mn, Fe, Co and Ni. It is found that the change in structure from the Ti_{1+x}Os_{2-x}RuB₂-type structure (*P6̄2m*, no. 189) to the Ti_{1+x}Rh_{2-x+y}Ir_{3-y}B₃-type (*Pbam*, no. 55) leads to a change of B₄ shape from trigonal planar B₄ (M = V-Mn) to zigzag B₄ fragment (M = Mn-Ni). Even though there is no group-subgroup relationship between the two structures, we present how the Ti_{1+x}Os_{2-x}RuB₂-type structure can easily be geometrically derived from the Ti_{1+x}Rh_{2-x+y}Ir_{3-y}B₃-type.

Keywords: Borides; trigonal planar B₄; trans zigzag B₄; ladders; chains of triangles

Introduction

Metal borides are known for some set of characteristic properties such as high melting points, superior hardness, and chemical inertness that originate from their extraordinary crystal chemistry, in which strong boron--boron and metal--boron bonds play a key role.^[1-10] The crystal chemistry of metal-rich borides has been enriched in recent years by the discovery of complex phases in which different boron fragments such as B₂, B₃, B₄, B₅ and B₆ were found.^[11-15] In some cases, these compounds exhibit highly exciting properties: Superconductivity was observed in NbRuB (containing B₂ dumbbells)^[16], in TaRuB and NbOsB (both containing zigzag B₄ units)^[17], while itinerant ferrimagnetism was reported for TiCrIr₂B₂ (trigonal planar B₄ units)^[18], itinerant ferromagnetism in arc-melted Nb₆Fe_{1-x}Ir_{6+x}B₈ (B₆ rings)^[19] which becomes an itinerant ferrimagnet when annealed at 1600 °C^[20]. Most of these boron fragments can be derived from the honeycomb boron layer of the AlB₂-type structure^[3]. Accordingly, the fragments arise from boron-centered trigonal metal prisms sharing a rectangular face, thus leading to short boron-boron distances (typically 1.7 to 1.8 Å). For fragments with more than three boron atoms, different configurations are possible such as for the B₄ (zigzag-B₄ in Mo₂IrB₂^[21] and Ti_{1+x}Rh_{2-x+y}Ir_{3-y}B₃ types^[22], bent-B₄ in β-Cr₂IrB₂^[13] or trigonal planar B₄ unit in the hexagonal Ti_{1+x}Os_{2-x}RuB₂ (*P* $\bar{6}2m$, no. 189)^[23]. Recently, weak spin frustration and ferrimagnetic ordering below 275 K was found in TiCrIr₂B₂ (Ti_{1+x}Os_{2-x}RuB₂-type) and attributed to the unique substructure of the magnetic element, namely a chain of equilateral Cr₃ triangles^[18] which strongly interacts with trigonal planar B₄ units. The discovery of this phase was the result of our increased efforts of designing new phases by incorporation of magnetic 3*d* elements into new boride structures. Naturally, after discovering TiCrIr₂B₂, the next target was to study the substitution of Cr by other 3*d* transition metals and its impact on the crystal structure and possibly magnetic properties. In the present work we report on the new boride series Ti_{2-x}M_{1+x-δ}Ir_{3+δ}B₃ (*x* = 0.5 for M = V-Mn, *x* = 0 for Mn-Ni and δ < 0.2) in which a structural change occurs by successive substitution of the 3*d* transition metal M = V, Cr, Mn, Fe, Co and Ni. Finally, we explain how the

Ti_{1+x}Os_{2-x}RuB₂-type (with trigonal planar B₄ fragment) and the Ti_{1+x}Rh_{2-x+y}Ir_{3-y}B₃-type (with zigzag B₄ fragment) structures can be geometrically derived from each other.

Experimental procedures

The boride phases were synthesized by a high temperature reaction in an electric arc furnace directly from the elements (more details on the synthesis can be found in the SI). Overall, three sets of samples were prepared with the starting compositions 2Ti:*M*:3Ir:3B, 1.5Ti:1.5*M*:3Ir:3B and Ti:2*M*:3Ir:3B, where *M* = V, Cr, Mn, Fe, Co or Ni. These three sets were prepared in order to investigate if the Ti:*M* ratio affects the type of boride obtained. Powders of the respective elements are mixed thoroughly in the corresponding ratio and pressed into dense pellets. The pellets are then arc-melted several times in the arc furnace (20 V voltage and 20 A applied current) which is filled with Ar. Small gray beads with metallic luster were obtained. Their weight was compared to the initial weight to keep track of any material lost during the reaction, but the loss turned out to be negligible. All samples were stable in air even after a long exposure time.

The beads were crushed, and single crystals were isolated from the powders under an optical microscope. The samples were then finely ground in an agate mortar and used to collect powder X-ray diffraction (PXRD) data, utilizing Cu K_α radiation ($\lambda = 1.54059 \text{ \AA}$) of a Stadi P powder diffractometer (STOE & Cie GmbH, Darmstadt, Germany) equipped with a Ge monochromator and an Image-plate detector. Each measurement took 3h and covered a 2Θ range from 10° to 90°. The powder diffraction data was refined by a full-matrix least-squares refinement (Rietveld) as implemented in the FULLROF Suite ^[24,25].

In case suitable single crystals were isolated, they were subsequently used to collect single-crystal X-ray diffraction (SCXRD) data, utilizing Mo-K_{α1} radiation ($\lambda = 0.709 \text{ \AA}$) of a Smart APEX diffractometer by Bruker equipped with a CCD detector. The structure was solved by direct methods using the SHELXS package and a full-matrix least-squares refinement was performed using SHELXL ^[26,27]. Additionally, the

presence of the metals in the single crystals were confirmed by energy dispersive X-ray spectroscopy (EDX) with a LEO 1450VP electron microscope from Carl ZEISS,

Results and Discussion

Phase analysis

In the powder diffraction data of all V- and Cr-containing samples the $\text{Ti}_{1+x}\text{Os}_{2-x}\text{RuB}_2$ -type phase was identified. However, these samples contained additional compounds, mainly the Cu_3Au -type $\text{TiIr}_3\text{B}_{1-y}$ phase ^[28] in all of them and the τ -boride $\text{Cr}_{7.9}\text{Ir}_{14.1}\text{B}_6$ ^[13] for the two Cr samples with higher Cr-content (Ti:M = 1 and $\frac{1}{2}$). For the Mn-containing samples with low Mn-content (Ti:M = 2 and 1), a structure change was observed as the $\text{Ti}_{1+x}\text{Rh}_{2-x+y}\text{Ir}_{3-y}\text{B}_3$ -type phase ^[22] was obtained as main product, while for higher Mn-content (Ti:M = $\frac{1}{2}$) only a minority $\text{Ti}_{1+x}\text{Os}_{2-x}\text{RuB}_2$ -type phase ^[23] is present, the main phase being the τ -boride (($\text{Fe}_{0.54}\text{Ir}_{0.46}$)₂₀ Fe_3B_6 -type) ^[29]. The $(\text{Ti}_{1-x}\text{Fe}_x)_3\text{Ir}_3\text{B}_3$ samples contain a $\text{Ti}_{1+x}\text{Rh}_{2-x+y}\text{Ir}_{3-y}\text{B}_3$ -type boride phase together with a τ -boride (($\text{Fe}_{0.54}\text{Ir}_{0.46}$)₂₀ Fe_3B_6 -type) ^[29] for all Ti:M ratios, and a third phase ($\text{TiIr}_3\text{B}_{1-y}$) ^[28] is found only for Ti:M = 2. The $(\text{Ti}_{1-x}\text{M}_x)_3\text{Ir}_3\text{B}_3$ samples with $M = \text{Co}$ and Ni contain a $\text{Ti}_{1+x}\text{Rh}_{2-x+y}\text{Ir}_{3-y}\text{B}_3$ -type boride only for Ti:M = 2. In these samples, some unindexed peaks are present, thus the weight fractions given in **Tables S1, S2 and S3** (supporting information, SI) are just relative values.

Single-crystal structure determination

In order to refine the proper compositions of the new phases, single-crystal refinements coupled with EDX analyses were carried out. Due to the irregular shapes of the single crystals studied by EDX only qualitative measurements were possible, except for the orthorhombic Mn-based phase which yielded the metal ratio 2.4(2):0.7(2):2.9(2) for Ti:Mn:Ir, which is in fair agreement with the results obtained from single-crystal diffraction below. The crystallographic and structure refinement data are given in **Tables 1 and 2**, while **Tables 3, S4, S5, S6 and S7** contain the refined atomic positions

and displacement parameters and **Table 4** contain selected bond lengths (for a representative of each structure type).

TiM₂Ir₂B₂ (*M* = V, Mn): The structure of Ti_{1+x}Os_{2-x}RuB₂ ^[23] was used as model for the refinement of single-crystal data of the V- and Mn-based compounds since the PXRD data indicated isotypism of both compounds with Ti_{1+x}Os_{2-x}RuB₂. From the TiOs₂RuB₂ model, Os was substituted by Ir and Ru by *M* (V, Mn) leading to TiM₂Ir₂B₂ as the starting model. The refinements converged in both cases smoothly. Since Ti and V cannot be distinguished using XRD (both are 1 electron apart and have similar atomic radius) and because EDX analysis had confirmed the presence of the two elements in the single crystal analyzed, the Ti- and V-sites were refined with a fixed 50:50 (Ti:V) mixed occupancy, thus the composition of this phase should be viewed as (Ti_{1-x}V_x)₂Ir₂B₂. In the case of *M* = Mn, the large difference in atomic radius between Ti and Mn was enough to differentiate both elements (similar to the reported *M* = Cr) ^[18]. However, disorder of Mn and Ir on the Mn site with the heavier Ir (8%) was necessary to fully occupy the site, leading to the refined chemical formula TiMn_{0.92(2)}Ir_{2.08(2)}B₂. Occupational disorder between a first-row transition metal and a 4*d* or 5*d* metal is frequently observed in metal borides such as Nb₆Fe_{1-x}Ir_{6+x}B₈ or (Fe_{0.54}Ir_{0.46})₂₀Fe₃B₆ ^[19,29]. Furthermore, the B–B distance had to be restrained to 1.85 Å (average B–B distance in Ti₂MnIr₃B₃, see below) as the refined distance was very large (2.22 Å), exceeding all other distances (1.75 – 1.90 Å) found for all B₄ units in this and related structure types.

Ti₂M₂Ir₃B₃ (*M* = Mn, Fe, Co, Ni): PXRD data established isotypism of these four compounds with Ti_{1+x}Rh_{2-x+y}Ir_{3-y}B₃-type structure. Suitable single crystals could be isolated in all cases, and the composition “Ti_{1+x}(Rh_{1-x})(Rh_{1+y})Ir_{3-y}B₃” was used as the starting model but replacing (Rh_{1-x}) and (Rh_{1+y}) by Ti and *M*, respectively, leading to the ideal starting formula Ti₂M₂Ir₃B₃. In all cases, the refinements converged smoothly. However, a mixed occupancy on the *M* site with the heavier Ir was necessary to fully occupy the *M* site, leading to the general chemical formula Ti₂M_{1-y}Ir_{3+y}B₃ (*y* < 0.2). The B–B bond lengths range from 1.81(5) Å to 1.90(5) Å for the outer B₇–B₈ bond and from 1.76(6) Å to 1.84(6) Å for the central B₈–B₈ bond of the zigzag B₄ fragment. A list of the bond lengths for all compounds can be found

in Tables S8 and S9 in the SI. In general, they fall into the expected range for intermetallic borides. The M–B and Ir–B bonds are roughly between 2.2 Å and 2.3 Å, while the Ti–B distances are mostly 2.4 Å or longer.

Structural descriptions

(Ti_{1-x}V_x)₂Ir₂B₂ and TiMn_{0.92(2)}Ir_{2.08(2)}B₂: All atoms are distributed in two layers at $z = 0$ and $z = 0.5$ along the c direction. All Ir atoms are found in the layer at $z = 0.5$ together with two out of three boron atoms (**Figure 1**). The two boron atoms (B1 and B2) build trigonal planar B₃ units with a B–B distance of 1.78(5) Å in (Ti_{1-x}V_x)₂Ir₂B₂ and 1.85 Å in TiMn_{0.92(2)}Ir_{2.08(2)}B₂. The layer at $z = 0$ contains all other metals (Ti, Mn, Ti/V) and the third boron atom (B3). In this layer the M (Ti/V or Mn) atoms form equilateral triangles with a M–M distance of 2.72(2) Å ($M = \text{Ti/V}$) or 2.61(1) Å ($M = \text{Mn}$). Two M₃ triangles are stacked on top of each other, forming M₃ chains with an intrachain distance corresponding to the c lattice parameter at ca. 3.19 Å. The shortest distance between two Mn–atoms of two adjacent triangles in the same layer is 6.404(7) Å, which is more than twice as large as the distance in the c direction. These distances and the boron–metal and metal–metal distances are comparable to those found in TiCrIr₂B₂ and reported Ti_{1+x}Os_{2-x}RuB₂-type phases such as Ti_{1.6}Os_{2.4}B₂ and Ti_{1-x}Fe_xOs₂RhB₂ ($0 < x < 0.5$).^[30] All atoms at $z = 0$ are coordinated by prisms build by atoms in the $z = 0.5$ layers: trigonal prisms for boron and pentagonal prisms for Ti and M (**Figure 1a**). Likewise, the boron atoms at $z = 0.5$ are coordinated by prisms of metals at $z = 0$, whereas the iridium atoms are coordinated by strongly distorted icosahedra of all atom. For clarity reasons, we will use the simplified formula TiM₂Ir₂B₂ in the following discussion to represent these two phases.

The TiMnIr₂B₂-phase contains a magnetically active element (Mn), thus the Mn substructure (chains of Mn₃ triangles) has the potential to produce interesting magnetic properties. Unfortunately, only 6 wt.-% of this phase has been synthesized until now, so the magnetic properties cannot be studied at this time. Nevertheless, comparing this substructure with other will lead to a better understanding of the potential magnetic properties. For example, the similar Cr substructure has produced the isomorphous TiCrIr₂B₂

ferrimagnet. Another boride phase containing a similar substructure of a magnetic element is NbFeB (ZrNiAl-type structure)^[31], also crystallizes in the hexagonal space group ($P\bar{6}2m$, no 189, Pearson symbol hP9) and contains trigonal boron-centered M_6B prisms. Thus, both structure types contain triangles of magnetic 3d transition metals. In contrast to the boron capped M_6B ($M = \text{Cr}, \text{Mn}$) prisms, the rectangular faces of the Fe_6B prisms in NbFeB are capped by Nb-atoms, resulting in isolated B atoms in the latter compound instead of trigonal B_4 fragments as found in $\text{TiM}\text{Ir}_2\text{B}_2$. Nevertheless, the M_3 ($M = \text{Cr}, \text{Mn}, \text{Fe}$) triangles in these three compounds are very similar, having comparable intra-triangle distances of 2.64 Å (in Cr_3), 2.61 Å (in Mn_3) and 2.67 Å (in Fe_3) as well as similar inter-triangle distances of 3.18 Å ($\text{Fe}_3 - \text{Fe}_3$), 3.19 Å ($\text{Mn}_3 - \text{Mn}_3$) and 3.22 Å ($\text{Fe}_3 - \text{Fe}_3$). Consequently, the distances within the chains of M_3 triangles in these three compounds are nearly the same, but the distance between these chains is structure-type dependent: The interchain distance of 8.61 Å in $\text{TiMnIr}_2\text{B}_2$ is similar to that in $\text{TiCrIr}_2\text{B}_2$ (8.55 Å), whereas it is only 6.01 Å in NbFeB (both center-to-center), hinting at different magnetic properties for these two structure types despite the similar magnetic chains of M_3 triangles. Such studies of magnetic properties would be highly interesting both experimentally and theoretically, as they would help shed some light on the effects of different interchain distances.

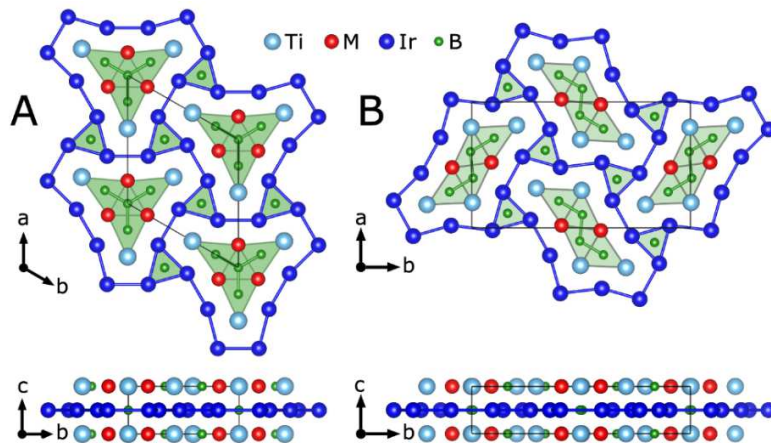


Figure 1. Projections of the structures of (a) $\text{TiM}\text{Ir}_2\text{B}_2$ ($M = \text{V}, \text{Mn}$; $\text{Ti}_{1+x}\text{Os}_{2-x}\text{RuB}_2$ -type) and of (b) $\text{Ti}_2\text{M}_{1-x}\text{Ir}_{3+x}\text{B}_3$ ($x < 0.2$; $M = \text{Mn-Ni}$; $\text{Ti}_{1+x}\text{Rh}_{2-x+y}\text{Ir}_{3-y}\text{B}_3$ -type) phases along [001] on top and along [100] at the bottom. The highlighted green triangles indicate boron-filled trigonal prisms. Note that for the $M = \text{V}$ phase, the Ti and M positions are all filled by the mixed Ti/V atoms.

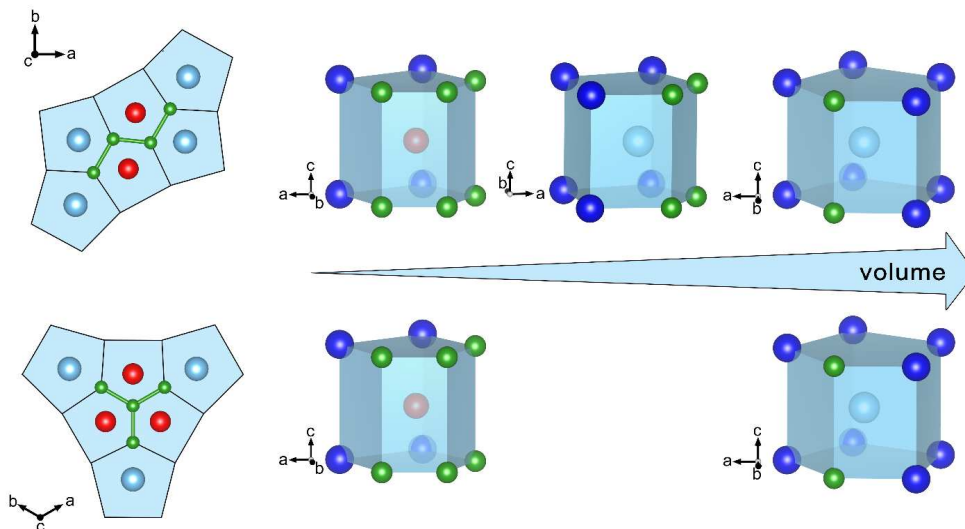


Figure 2. Sets of pentagonal prisms centered by M (red) and Ti (cyan) in the orthorhombic $\text{Ti}_{1+x}\text{Rh}_{2-x+y}\text{Ir}_{3-y}\text{B}_3$ -type structure (top) and the hexagonal $\text{Ti}_{1+x}\text{Os}_{2-x}\text{RuB}_2$ -type structure (bottom).

$\text{Ti}_2\text{M}_{1-x}\text{Ir}_{3+x}\text{B}_3$ ($x < 0.2$; $M = \text{Mn-Ni}$): Analogous to the $\text{Ti}_{1+x}\text{Os}_{2-x}\text{RuB}_2$ -type structure discussed above, the structure of $\text{Ti}_2\text{M}_{1-x}\text{Ir}_{3+x}\text{B}_3$ compounds ($\text{Ti}_{1+x}\text{Rh}_{2-x+y}\text{Ir}_{3-y}\text{B}_3$ -type) displays two different layers at $z = 0$ and $z = 0.5$: Ti, M and isolated boron atoms are found at $z = 0$, while Ir and other B atoms (building zigzag B_4 fragments) fill the $z = 0.5$ layer.

Two M_2 dumbbells and two Ti atoms form a trigonal prism ($[\text{Ti}_2\text{M}_4]\text{B}_8$ prism) which is centered by the inner B atom (B_8) of the zigzag B_4 fragment. The outer B atoms (B_7) of the zigzag B_4 fragment resides in the nearby trigonal prisms which have the inverse Ti: M ratio ($[\text{Ti}_4\text{M}_2]\text{B}_7$ prisms). The zigzag B_4 fragment arises from the rectangular face sharing of $[\text{Ti}_2\text{M}_4]\text{B}_8$ and $[\text{Ti}_4\text{M}_2]\text{B}_7$ prisms (**Figure 1b**). The two other rectangular faces of these prisms are all capped by Ir atoms at $z = 0.5$. Six of those Ir atoms form another set of trigonal prisms centered by the isolated B_9 atoms ($[\text{Ir}_6]\text{B}_9$ prism). Because the two layers at $z = 0$ and $z = 0.5$ alternate along the c -axis, all trigonal prisms form infinite columns parallel to $[001]$ by sharing their trigonal faces. Just as in the previous structure type, all atoms at $z = 0$ are coordinated by prisms build by atoms in the $z = 0.5$ layers including pentagonal prisms for Ti and M (**Figures 1 and 2**). In contrast, only the boron atoms at $z = 0.5$ are coordinated by prisms of metals at $z = 0$, whereas the iridium atoms are

coordinated by strongly distorted icosahedra of all atom types as previously described in $\text{Ti}_{1+x}\text{Rh}_{2-x+y}\text{Ir}_{3-y}\text{B}_3$ [22]. The B–B distance in this series varies from 1.81(4) Å for $M = \text{Ni}$ to 1.90(4) Å for $M = \text{Mn}$. These phases are the first of this structure type containing a magnetic element (M), thus it is important to describe the substructure build by M : The shortest M – M distance, which is very similar in all phases and varies from 2.61(1) Å for $M = \text{Mn}$ and Ni to 2.67(1) Å for $M = \text{Fe}$ and Co , is consistent with M_2 dumbbells. The distance between dumbbells (inter-dumbbell distance) has the same length as the c lattice parameter (ca. 3.23 Å), thereby building a ladder substructure (M_2 chain). A similar ladder-like arrangement of magnetic Fe atoms (with Fe–Fe distances of 2.49 Å and 2.97 Å) has been observed in $\text{Ti}_9\text{Fe}_2\text{Ru}_{18}\text{B}_8$, and it is believed to have induced ferromagnetism in this phase [32]. However, the significant differences between these two types of ladder substructures (ca. 0.2 Å larger distances in the new substructure) can affect the magnetic properties. In particular, the proximity of the nearby B_4 fragments which strongly interact with the new ladders (**Figure 3b**) in the new phases (absent in $\text{Ti}_9\text{Fe}_2\text{Ru}_{18}\text{B}_8$, **Figure 3c**) may drastically impact the magnetic properties, as strong bonding between M and B will lower the electron density on M and thus reduce the strength of M – M magnetic interactions (a related manuscript on theoretical calculations will be communicated soon).

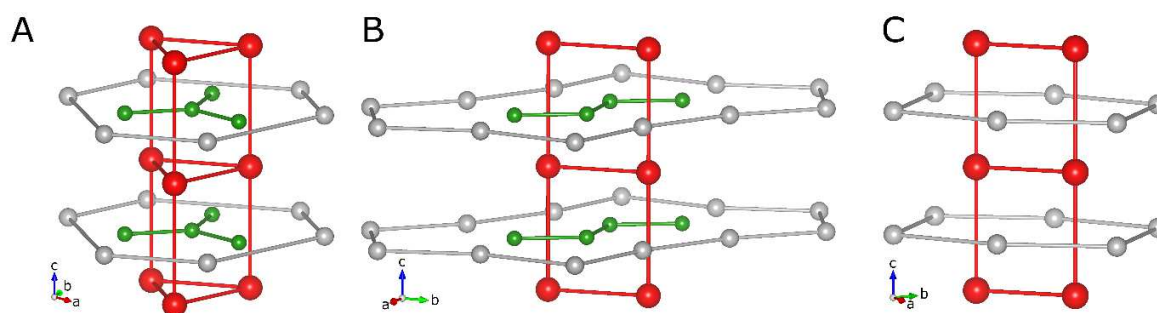


Figure 2. Detailed view of the different M –substructures and coordination found in (a) the hexagonal TiMIR_2B_2 structure ($\text{Ti}_{1+x}\text{Os}_{2-x}\text{RuB}_2$ –type), (b) in the orthorhombic $\text{Ti}_2\text{MIR}_3\text{B}_3$ structure ($\text{Ti}_{1+x}\text{Rh}_{2-x+y}\text{Ir}_{3-y}\text{B}_3$ –type, right) and in the tetragonal $\text{Ti}_9\text{M}_2\text{Ru}_{18}\text{B}_8$ ($M = \text{Fe}$) structure.

Structural relationship between $\text{Ti}_{1-x}\text{Rh}_{2-x+y}\text{Ir}_{3-y}\text{B}_3$ – and $\text{Ti}_{1-x}\text{Os}_{2-x}\text{RuB}_2$ –type structures

Using different *3d* transition metals for *M* (*M* = V - Ni) in the series $(\text{Ti}_{1-x}\text{M}_x)_3\text{Ir}_3\text{B}_3$ ($x = 1/3, 1/2$) results in the formation of hexagonal $\text{Ti}_{1-x}\text{Os}_{2-x}\text{RuB}_2$ -type structure for *M* = V, Cr and Mn on the one hand and of orthorhombic $\text{Ti}_{1-x}\text{Rh}_{2-x+y}\text{Ir}_{3-y}\text{B}_3$ -type structure for *M* = Mn, Fe, Co and Ni on the other hand. Moreover, in the case of *M* = Mn, both structures occur side by side. Comparing the two structure types, a close relationship between them becomes apparent: Both are layered along the *c*-axis, both have a metal-to-boron ratio *M*:B of 2:1 and both contain isolated boron as well as B_4 fragments. However, the B_4 unit is trigonal planar in the $\text{Ti}_{1-x}\text{Os}_{2-x}\text{RuB}_2$ -type structure while it is zigzag shaped in the $\text{Ti}_{1-x}\text{Rh}_{2-x+y}\text{Ir}_{3-y}\text{B}_3$ -type structure. Each boron atom of both B_4 -units is located inside a trigonal prism made from *M* and Ti. The different topology of the B_4 -fragment and ultimately the different space group symmetry of the structures depends only on how those trigonal prisms are connected. While three trigonal prisms in the $\text{Ti}_{1-x}\text{Os}_{2-x}\text{RuB}_2$ -type structure are connected via one of their rectangular faces to a central trigonal prism, the trigonal prisms in the $\text{Ti}_{1-x}\text{Rh}_{2-x+y}\text{Ir}_{3-y}\text{B}_3$ -type structure are all successively connected by their rectangular faces (**Figures 1 and 2**).

The close relationship between the two structures raises the question why one is preferred over the other. By looking at the whole series one finds that for the larger *3d* transition metals (V, Cr, Mn) the hexagonal structure is preferred, while the smaller *3d* metals (Mn, Fe, Co, Ni) prefer the orthorhombic structure. Analyzing the coordination polyhedra (**Figure 2**) around the metal atoms *M* and Ti, two different polyhedra exist for the hexagonal structure while three different polyhedra occur in the orthorhombic structure. Two out of three polyhedra of the orthorhombic structure are identical with the two polyhedra of the hexagonal structure. Accordingly, the orthorhombic structure contains a coordination polyhedron that does not exist in the hexagonal structure; thus, this explains the absence of a group-subgroup relationship between them.

The polyhedra have different volumes (**Figure 2**), and the volume increases with decreasing number of boron atoms being part of the coordination polyhedron. The hexagonal structure contains the small polyhedron (six boron atoms participating) and the large polyhedron (two boron atoms involved). In the

orthorhombic structure, however, an additional third coordination polyhedron exists and contains four boron atoms; thus, its volume lies in-between the previous two.

Naturally, we expect the large atoms to occupy the larger polyhedron, as it was found in the hexagonal structure of $\text{TiCrIr}_2\text{B}_2$, where Ti seats in the larger polyhedron while the smaller Cr atom occupies the smaller polyhedron. The same holds true for the hexagonal compounds with $M = \text{V}$ and Mn .

Due to the presence of three different polyhedra, the situation is slightly more complex in the orthorhombic structures, but the general trend is the same. The Ti atoms occupy the large and the intermediate polyhedra, while the smaller M atoms ($M = \text{Mn}, \text{Fe}, \text{Co}$ or Ni) are found inside the small polyhedron mixed with a small amount of Ir (the second largest metal atom, $r_{\text{Ti}} > r_{\text{Ir}} > r_M$).

The two different pentagonal prisms of the hexagonal structure occur three times each, while the three different pentagonal prisms of the orthorhombic structure occur twice each. Thus, the total number of pentagonal prisms is the same for both structures. Consequently, the ratio between the number of large sites (preferred by Ti) to the number of small sites (preferred by M) in the hexagonal structure is 1:1. In comparison, the ratio between the number of sites preferred by Ti to the number of sites preferred by M in the orthorhombic structure is 2:1, hinting at larger unit cells for the orthorhombic structure. Indeed, the average cell volume is 406.5 \AA^3 for the hexagonal compounds and 415.8 \AA^3 for the orthorhombic compounds.

As mentioned above, a group-subgroup relationship does not exist between the two structure types. Nevertheless, starting from the orthorhombic structure, one can derive the hexagonal structure with the following simple steps:

- 1) Identify two similar hexagonal unit cells (**Figure 4, left, red shadings**) within the orthorhombic $\text{Ti}_{1+x}\text{Rh}_{2-x+y}\text{Ir}_{3-y}\text{B}_3$ -type unit cell (**Figure 4, left, yellow shadings**),
- 2) Rotate one hexagonal unit cell (**Figure 4, left, blue outline**) by 180° around the c -axis, which produces the other adjacent hexagonal unit cell, and

- 3) Shift the rotated left hexagonal unit with respect to the other hexagonal cell along a by ca. 1.8 \AA (blue arrow).
- 4) The hexagonal $\text{Ti}_{1+x}\text{Os}_{2-x}\text{RuB}_2$ -type structure is obtained (**Figure 4, right**).

No modification in c direction is required because of the same layered arrangement of both structures. This transformation can be considered as a form of glide-reflection twinning of the hexagonal structure [33].

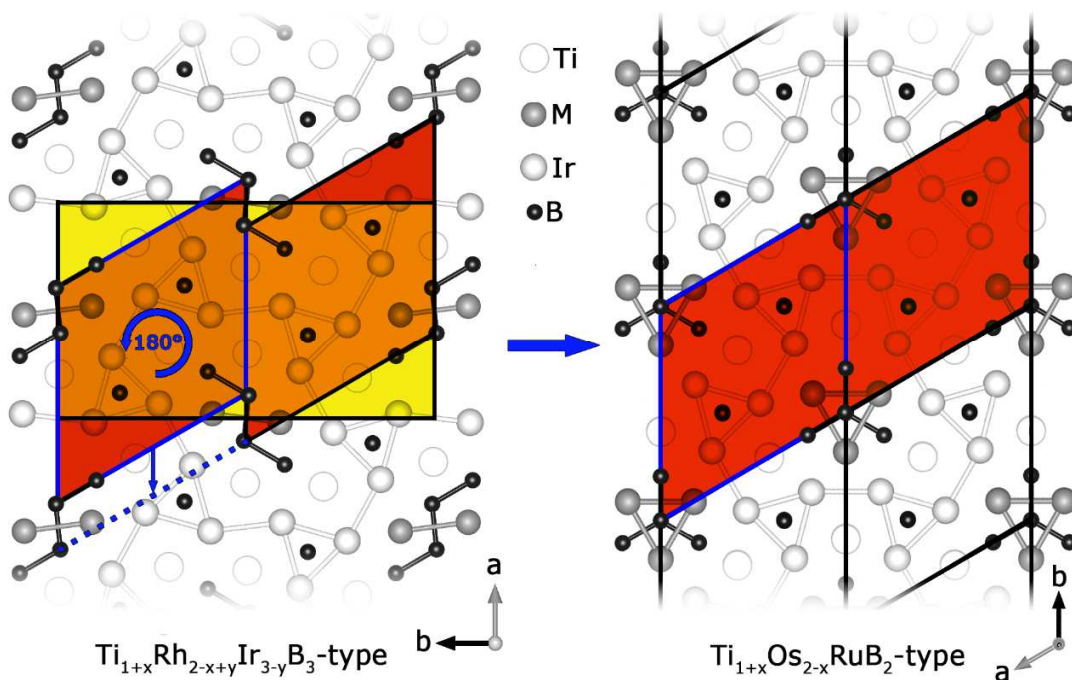


Figure 4: structural relation between the orthorhombic $\text{Ti}_{1+x}\text{Rh}_{2-x+y}\text{Ir}_{3-y}\text{B}_3$ -type structure (left, unit cell shaded in yellow) and the hexagonal $\text{Ti}_{1+x}\text{Os}_{2-x}\text{RuB}_2$ -type structure (right, unit cells shaded in red).

Conclusion

We have synthesized and fully characterized new phases within the series $\text{Ti}_{2-x}\text{M}_{1+x-\delta}\text{Ir}_{3+\delta}\text{B}_3$ ($x = 0.5$ for $M = \text{V-Mn}$, $x = 0$ for $M = \text{Mn-Ni}$ and $\delta < 0.2$), the main product is isostructural to hexagonal $\text{Ti}_{1+x}\text{Os}_{2-x}\text{RuB}_2$ for $M = \text{V-Mn}$, while for $M = \text{Fe, Co or Ni}$ the $\text{Ti}_{1+x}\text{Rh}_{2-x+y}\text{Ir}_{3-y}\text{B}_3$ -type structure is adopted, independent of the Ti:M ratio of the starting composition. For $M = \text{Mn}$, both structures were

obtained side by side. The different Ti:M ratio (1:1 in the hexagonal and 2:1 in the orthorhombic) is attributed to differently sized polyhedra around these atoms, thereby directing the formation of each structure type. Moreover, the two structure types can be geometrically derived from each other, even though there is no obvious group–subgroup relationship.

Acknowledgements

This work was supported by the National Science Foundation Career award to BPTF (no. DMR-1654780) as well as UC Riverside (Dissertation Year Award for JPS).

References

1. Akopov G, Yeung MT, Kaner RB. Rediscovering the Crystal Chemistry of Borides. *Adv Mater.* 2017;29(21):1604506. doi:10.1002/adma.201604506
2. Ma T, Li H, Zheng X, et al. Ultrastrong Boron Frameworks in ZrB₁₂: A Highway for Electron Conducting. *Adv Mater.* 2017;29(3):1604003. doi:10.1002/adma.201604003
3. Scheifers JP, Zhang Y, Fokwa BPT. Boron: Enabling Exciting Metal-Rich Structures and Magnetic Properties. *Acc Chem Res.* 2017;50(9). doi:10.1021/acs.accounts.7b00268
4. Yeung MT, Lei J, Mohammadi R, et al. Superhard Monoborides: Hardness Enhancement through Alloying in W_{1-x}Ta_xB. *Adv Mater.* 2016;28(32):6993-6998. doi:10.1002/adma.201601187
5. Petsagkourakis I, Tybrandt K, Crispin X, Ohkubo I, Satoh N, Mori T. Thermoelectric materials and applications for energy harvesting power generation. *Sci Technol Adv Mater.* 2018;19(1):836-862. doi:10.1080/14686996.2018.1530938
6. Rau JV, Latini A. New Hard and Superhard Materials: RhB_{1.1} and IrB_{1.35}. *Chem Mater.* 2009;21(8):1407-1409. doi:10.1021/cm900310j

7. Albert B, Hillebrecht H. Boron: Elementary Challenge for Experimenters and Theoreticians. *Angew Chemie Int Ed.* 2009;48(46):8640-8668. doi:10.1002/anie.200903246
8. Levine JB, Tolbert SH, Kaner RB. Advancements in the Search for Superhard Ultra-Incompressible Metal Borides. *Adv Funct Mater.* 2009;19(22):3519-3533. doi:10.1002/adfm.200901257
9. Gu Q, Krauss G, Steurer W. Transition Metal Borides: Superhard versus Ultra-incompressible. *Adv Mater.* 2008;20(19):3620-3626. doi:10.1002/adma.200703025
10. Chung HY, Weinberger MB, Levine JB, et al. Synthesis of ultra-incompressible superhard rhenium diboride at ambient pressure. *Science (80-)*. 2007;316(5823):436-439. doi:10.1126/science.1139322
11. Mbarki M, Touzani R St., Fokwa BPT. Experimental and Theoretical Investigations of the Ternary Boride NbRuB with a Layerlike Structure Type. *Eur J Inorg Chem.* 2014;2014(8):1381-1388. doi:10.1002/ejic.201301488
12. Jedlicka H, Benesovsky F, Nowotny H. Die Kristallstruktur des W₃CoB₃ und der dazu isotypen Phasen Mo₃CoB₃, Mo₃NiB₃ und W₃NiB₃. *Monatshefte für Chemie.* 1969;100(3):844-850. doi:10.1007/BF00900567
13. Kotzott D, Ade M, Hillebrecht H. Synthesis and crystal structures of α - and β -modifications of Cr₂IrB₂ containing 4-membered B₄ chain fragments, the τ -boride Cr_{7.9}Ir_{14.1}B₆ and orthorhombic Cr₂B. *Solid State Sci.* 2008;10(3):291-302. doi:10.1016/j.solidstatesciences.2007.09.014
14. Ade M, Kotzott D, Hillebrecht H. Synthesis and crystal structures of the new metal-rich ternary borides Ni₁₂AlB₈, Ni₁₂GaB₈ and Ni_{10.6}Ga_{0.4}B₆-examples for the first B₅ zig-zag chain fragment. *J Solid State Chem.* 2010;183(8):1790-1797. doi:10.1016/j.jssc.2010.05.009
15. Fokwa BPT, Hermus M. All-Boron Planar B₆ Ring in the Solid-State Phase Ti₇Rh₄Ir₂B₈. *Angew*

Chemie Int Ed. 2012;51(7):1702-1705. doi:10.1002/anie.201106798

16. Xie W, Luo H, Baroudi K, Krizan JW, Phelan BF, Cava RJ. Fragment-Based Design of NbRuB as a New Metal-Rich Boride Superconductor. *Chem Mater.* 2015;27(4):1149-1152.
doi:10.1021/cm504449s
17. Zheng Q, Gumeniuk R, Rosner H, et al. Synthesis, crystal structure and properties of the new superconductors TaRuB and NbOsB. *J Phys Condens Matter.* 2015;27(41):415701.
doi:10.1088/0953-8984/27/41/415701
18. Küpers M, Lutz-Kappelman L, Zhang Y, Miller GJ, Fokwa BPT. Spin Frustration and Magnetic Ordering from One-Dimensional Stacking of Cr₃ Triangles in TiCrIr₂B₂. *Inorg Chem.* 2016;55(11):5640-5648. doi:10.1021/acs.inorgchem.6b00714
19. Mbarki M, St. Touzani R, Fokwa BPT. Unexpected Synergy between Magnetic Iron Chains and Stacked B₆ Rings in Nb₆Fe_{1-x}Ir_{6+x}B₈. *Angew Chemie Int Ed.* 2014;53(48):13174-13177.
doi:10.1002/anie.201406397
20. Sharma N, Mbarki M, Zhang Y, Huq A, Fokwa BPT. Structural-Distortion-Driven Magnetic Transformation from Ferro- to Ferrimagnetic Iron Chains in B₆-based Nb₆FeIr₆B₈. *Angew Chemie Int Ed.* 2018;57(32):10323-10327. doi:10.1002/anie.201804841
21. Rogl P, Benesovsky F, Nowotny H. Über einige Komplexboride mit Platinmetallen. *Monatshefte für Chemie.* 1972;103(4):965-989. doi:10.1007/BF00905170
22. Goerens C, Fokwa BPT. The complex metal-rich boride Ti_{1-x}Rh_{2-xy}Ir_{3-y}B₃ (x=0.68, y=1.06) with a new structure type containing B₄ zigzag fragments: Synthesis, crystal chemistry and theoretical calculations. *J Solid State Chem.* 2012;192:113-119. doi:10.1016/j.jssc.2012.04.005
23. Fokwa BPT, Von Appen J, Dronskowski R. Synthesis of a missing structural link: The first trigonal planar B₄ units in the novel complex boride Ti_{1+x}Os_{2-x}RuB₂ (x = 0.6). *Chem Commun.* 2006;(42):4419-4421. doi:10.1039/b608903h

24. Rodríguez-Carvajal J. Recent advances in magnetic structure determination by neutron powder diffraction. *Phys B Condens Matter*. 1993;192(1-2):55-69. doi:10.1016/0921-4526(93)90108-I
25. Rodríguez-Carvajal J. FullProf: A Program for Rietveld Refinement and Profile Matching Analysis of Complex Powder Diffraction Patterns. In: *Satellite Meeting on Powder Diffraction of the XV Congress of the IUCr*. Toulouse; 1990:127.
26. Sheldrick GM. A short history of SHELX. *Acta Crystallogr Sect A Found Crystallogr*. 2008;64(1):112-122. doi:10.1107/S0108767307043930
27. Sheldrick GM. Crystal structure refinement with SHELXL. *Acta Crystallogr Sect C Struct Chem*. 2015;71:3-8. doi:10.1107/S2053229614024218
28. Eremenko VN, Shtepa TD, Sirotenko VG. Intermediate phases in alloys of titanium with iridium, rhodium, and osmium. *Sov Powder Metall Met Ceram*. 1966;5(6):487-490. doi:10.1007/BF00775541
29. Sologub O, Rogl P, Giester G. The tau-borides τ -(Fe_{0.54}Ir_{0.46})₂₀Fe₃B₆ and τ -(Co_{0.64}Ir_{0.36})₂₁Co_{0.16}B₄B₆. *Intermetallics*. 2010;18(4):694-701. doi:10.1016/j.intermet.2009.11.010
30. Fokwa BPT, Dronskowski R. New Transition-Metal Borides containing Trigonal-Planar B 4 - Units: Syntheses and Single-Crystal Structure Analyses of Ti_{1.6}Os_{2.4}B₂ and Ti_{1-x}Fe_xOs₂RhB₂. *Zeitschrift für Anorg und Allg Chemie*. 2008;634(11):1955-1960. doi:10.1002/zaac.200800219
31. Kuzma Y, Tsolkovskii T, Baburova O. The Systems Nb-Fe-B and Nb-Co-B. *Inorg Mater*. 1968;4(7):950-953.
32. Fokwa BPT, Samolyuk GD, Miller GJ, Dronskowski R. Ladders of a Magnetically Active Element in the Structure of the Novel Complex Boride Ti₉Fe₂Ru₁₈B₈: Synthesis, Structure, Bonding, and Magnetism. *Inorg Chem*. 2008;47(6):2113-2120. doi:10.1021/ic7020963

33. Hyde, B. G., Andersson, S., Bakker, M., Plug, C. M. & O'Keeffe, M. The (twin) composition plane as an extended defect and structure-building entity in crystals. *Progress in Solid State Chemistry* (1979) doi:10.1016/0079-6786(79)90002-5.

Table 1: Crystallographic and structure refinement data of $\text{Ti}_{1-x}\text{V}_x\text{Ir}_2\text{B}_2$ and $\text{TiMn}_{0.92(2)}\text{Ir}_{2.08(2)}\text{B}_2$ (obtained from the starting composition $\text{Ti}:2\text{Mn}:3\text{Ir}:3\text{B}$).

Formula	$\text{Ti}_{1-x}\text{V}_x\text{Ir}_2\text{B}_2$	$\text{TiMn}_{0.92(2)}\text{Ir}_{2.08(2)}\text{B}_2$
space group, Z	$P-62m$ (no. 189); 3	
formula weight (g/mol)	504.86	519.38
$F(000)$	627	645
lattice parameters		
a (Å)	8.601(2)	8.610(2)
b (Å)	8.601(2)	8.610(2)
c (Å)	3.1870(6)	3.1880(6)
V (Å ³)	204.18(6)	204.65(6)
calc. density (g/cm ³)	12.318	12.634
abs. coefficient (mm ⁻¹)	103.253	107.599
θ -range (°)	$4.74 < \theta < 35.69$	$4.74 < \theta < 35.78$
hkl -range	$-4 \leq h \leq 14$	$-13 \leq h \leq 14$
	$-14 \leq k \leq 13$	$-14 \leq k \leq 11$
	$-4 \leq l \leq 5$	$-4 \leq l \leq 5$
no. of reflections, R_{int}	1809; 0.0881	2166; 0.1373
indep. reflections	382	385
no. parameters	17	20
R_1 ; wR_2 (all I)	0.0639; 0.1037	0.0585; 0.1480
GooF	1.110	1.114
diff. peak / hole (e·Å ⁻³)	-3.583/ 4.406	-6.070 / 7.444

Table 2: Crystallographic and single-crystal structure data of $\text{Ti}_2M_{1-x}\text{Ir}_{3+x}\text{B}_3$ obtained from the starting composition $2\text{Ti}:M:3\text{Ir}:3\text{B}$ with $M = \text{Mn}, \text{Fe}$ and Co .

Formula	$\text{Ti}_2\text{Mn}_{0.83(1)}\text{Ir}_{3.17(1)}\text{B}_3$	$\text{Ti}_2\text{Fe}_{0.91(1)}\text{Ir}_{3.09(1)}\text{B}_3$	$\text{Ti}_2\text{Co}_{0.88(1)}\text{Ir}_{3.12(1)}\text{B}_3$	$\text{Ti}_2\text{Ni}_{0.88(1)}\text{Ir}_{3.12(1)}\text{B}_3$
space group, Z	<i>Pbam</i> (no. 55); 4			
formula weight (g/mol)	783.10	772.27	779.09	778.89
$F(000)$	1295	1281	1291	1295
lattice parameters				
a (Å)	8.639(2)	8.618(1)	8.60(2)	8.598(2)
b (Å)	15.004(4)	14.975(7)	15.00(3)	14.970(4)
c (Å)	3.228(7)	3.221(1)	3.225(5)	3.238(7)
V (Å ³)	418.4(9)	415.7(2)	416.0(2)	416.8(2)
calc. density (g/cm ³)	12.432	12.340	12.439	12.413
abs. coefficient (mm ⁻¹)	106.281	104.932	106.143	106.429
θ -range (°)	4.71 < θ < 35.93	5.46 < θ < 35.38	4.72 < θ < 35.76	4.72 < θ < 28.52
hkl -range	-12 ≤ h ≤ 14 -16 ≤ k ≤ 24 -4 ≤ l ≤ 5	-13 ≤ h ≤ 14 -8 ≤ k ≤ 24 -4 ≤ l ≤ 5	-11 ≤ h ≤ 14 -22 ≤ k ≤ 24 -4 ≤ l ≤ 5	-11 ≤ h ≤ 7 -19 ≤ k ≤ 20 -4 ≤ l ≤ 4
no. of reflections, R_{int}	4318; 0.1311	3320; 0.0681	4238; 0.1119	2331; 0.0934
indep. reflections	1082	1019	1063	618
no. parameters	46	37	46	41
R_1 ; wR_2 ($I > 2\sigma(I)$)	0.0588; 0.0912	0.0518; 0.0952	0.0610; 0.1133	0.0462; 0.1004
R_1 ; wR_2 (all I)	0.1111; 0.1045	0.0772; 0.1064	0.1103; 0.1294	0.0684; 0.1099
GooF	1.067	1.090	1.064	1.042
diff. peak / hole (e·Å ⁻³)	-5.427 / 7.830	-4.965 / 5.601	-5.896 / 5.794	-4.455 / 3.404

Table 3: Atomic coordinates, site occupation factors (SOF) and displacement parameters of $\text{TiMn}_{0.92(2)}\text{Ir}_{2.08(2)}\text{B}_2$ and $\text{Ti}_2\text{Ni}_{0.88(1)}\text{Ir}_{3.12(1)}\text{B}_3$. U_{13} and $U_{23} = 0$.

$\text{TiMn}_{0.92(2)}\text{Ir}_{2.08(2)}\text{B}_2$										
atom	Site	x	y	z	SOF	U_{eq}	U_{11}	U_{22}	U_{33}	U_{12}
Ir1	6k	0.4636(2)	0.2760(2)	0.5	1	0.0096(3)	0.0058(4)	0.0058(5)	0.0190(5)	0.0042(4)
Mn2/Ir2	3f	0.1786(7)	0.1786(7)	0	0.93(2)/ 0.07(2)	0.0010(2)	0.014 (2)	0.014(2)	0.005(2)	0.009(2)
Ti3	3f	0.4174(9)	0	0	1	0.005(1)	0.006(2)	0.003(2)	0.011(2)	0.003(2)
B1	1b	0	0	0.5	1	0.028(9)	-	-	-	-
B2	3g	0	0.258(9)	0.5	1	0.028(9)	-	-	-	-
B3	2c	0.6667	0.3333	0	1	0.028(9)	-	-	-	-
$\text{Ti}_2\text{Ni}_{0.88(1)}\text{Ir}_{3.12(1)}\text{B}_3$										
atom	Site	x	y	z	SOF	U_{eq}	U_{11}	U_{22}	U_{33}	U_{12}
Ir1	4h	0.0197(2)	0.09511(9)	0.5	1	0.0117(3)	0.0024(5)	0.0092(7)	0.0236(8)	0.0007(4)
Ir2	4h	0.7148(2)	0.14228(9)	0.5	1	0.0118(4)	0.0024(6)	0.0095(7)	0.0236(7)	-0.0009(4)
Ir3	4h	0.9337(2)	0.26982(9)	0.5	1	0.0129(4)	0.0029(5)	0.0097(7)	0.0262(8)	-0.0006(4)
Ir4/Ni4	4g	0.4748(4)	0.0858(2)	0	0.11(2)/ 0.89(2)	0.010(2)	0.006(2)	0.015 (2)	0.009 (2)	0.003(2)
Ti5	4g	0.1819(6)	0.2069(4)	0	1	0.0050(8)	0.005(2)	0.007(3)	0.002(3)	-0.001(2)
Ti6	4g	0.1985(6)	0.9962(4)	0	1	0.0050(8)	0.005(2)	0.007(3)	0.002(3)	-0.001(2)
B7	4h	0.290(4)	0.099(3)	0.5	1	0.010(4)	-	-	-	-
B8	4h	0.605(4)	0.006(3)	0.5	1	0.010(4)	-	-	-	-
B9	4g	0.890(4)	0.165(3)	0	1	0.010(4)	-	-	-	-

Table 4: Interatomic distances (Å) of $\text{TiMn}_{0.92(2)}\text{Ir}_{2.08(2)}\text{B}_2$ and $\text{Ti}_2\text{Ni}_{0.88(1)}\text{Ir}_{3.12(1)}\text{B}_3$.

$\text{TiMn}_{0.92(2)}\text{Ir}_{2.08(2)}\text{B}_2$		
Atom 1	Atom 2	d(atom1 – atom2) (Å)
B1	B2	2.22(6)
	Mn2	2.21(1)
B2	Mn2	2.10(4)
	Ti3	2.53(4)
	Ir1	2.14(2)
B3	Ir1	2.23(1)
	Ti3	2.59(1)
Ir1	Ir1	2.70(1) – 2.80(1)
Mn2	Mn2	2.61(1) – 3.19(1)
$\text{Ti}_2\text{Ni}_{0.88(1)}\text{Ir}_{3.12(1)}\text{B}_3$		
B7	B8	1.81(6)

B8	B8	1.81(4)
B7	Ir1-3	2.28(2) – 2.47(3)
	Ti5, Ti6 & Ir4/Ni4	2.32(3) – 2.33(3)
B8	Ir1-3	2.25(3)
	Ti5, Ti6 & Ir4/Ni4	2.23(2) – 2.34(2)
B9	Ir1-3	2.23(2) – 2.29(2)
	Ti5, Ti6 & Ir4/Ni4	2.53(4) – 2.62(4)
Ir1-3	Ir1-3	2.68(1) – 2.87(1)
Ir4/Ni4	Ir4/Ni4	2.61(1) – 3.22(1)
